ELSEVIER

Materials Characterization 52 (2004) 331–340

MATERIALS CHARACTERIZATION

A quantitative-metallographic study of the sintering behaviour of dolomite

H.A. Yeprem[a], E. Türedi[b], S. Karagöz[b,*]

[a]Department of Metallurgical and Materials Engineering, Yildiz Technical University, Istanbul, Turkey
[b]Department of Metallurgical and Materials Engineering, Kocaeli University, Veziroglu Campus, Izmit-Kocaeli 41040, Turkey

Received 24 April 2004; received in revised form 16 June 2004; accepted 17 June 2004

Abstract

Grain growth of the MgO phase during sintering of natural dolomite from Selcuklu-Konya in Turkey was studied in the temperature range 1600–1700 °C. For comparison purposes, iron oxide (98.66% mill scale) was added up to 1.5%. The compositions of the phases formed during sintering were studied using X-ray diffraction and scanning electron microscopy (SEM) with energy dispersive X-ray spectroscopy. Quantitative-metallographic analyses were performed on images taken by SEM. For the automatic image analysis of dolomite microstructures, material (atomic number) contrast with backscattered electrons (BSEs) was utilized because it yields higher phase contrast compared to secondary electrons (SEs).

Iron oxide additions to dolomite result in dense dolomite structures at given sintering temperatures, where phases with low melting temperatures are developed. During liquid phase sintering, periclase is enriched with iron, which destabilizes the MgO phase. The relevant kinetic exponents for MgO in the natural doloma and 0.5% Fe_2O_3 added doloma were 6 and 2, and the activation energies were 108 and 243 kJ/mol, respectively.

Keywords: Dolomite; MgO; Sintering; SEM; Grain growth

1. Introduction

Dolomite is a basic refractory raw material and consists of a mixture of calcium carbonate ($CaCO_3$) and magnesium carbonate ($MgCO_3$) [1]. After calcination, the material decomposes to lime (CaO) and periclase (MgO). Sintered dolomite (doloma) gains importance in the steel-making industry due to its high thermomechanical and erosion wear properties [2,3]. These properties are gained especially during sintering. For the stabilization of the doloma microstructure, raw dolomite is sintered with flux additions, e.g., mill scale (Fe_2O_3). In Fig. 1, the schematic microstructural development of dolomite with Fe_2O_3 addition during sintering is given. Sintering allows the formation of phases, like dicalciumferrite, tetracalciumaluminofer-

* Corresponding author. Tel.: +90-262-3353-658x120; fax: +90-262-3355-486.
E-mail address: karagoez@kou.edu.tr (S. Karagöz).

1044-5803/$ - see front matter © 2004 Elsevier Inc. All rights reserved.
doi:10.1016/j.matchar.2004.06.004

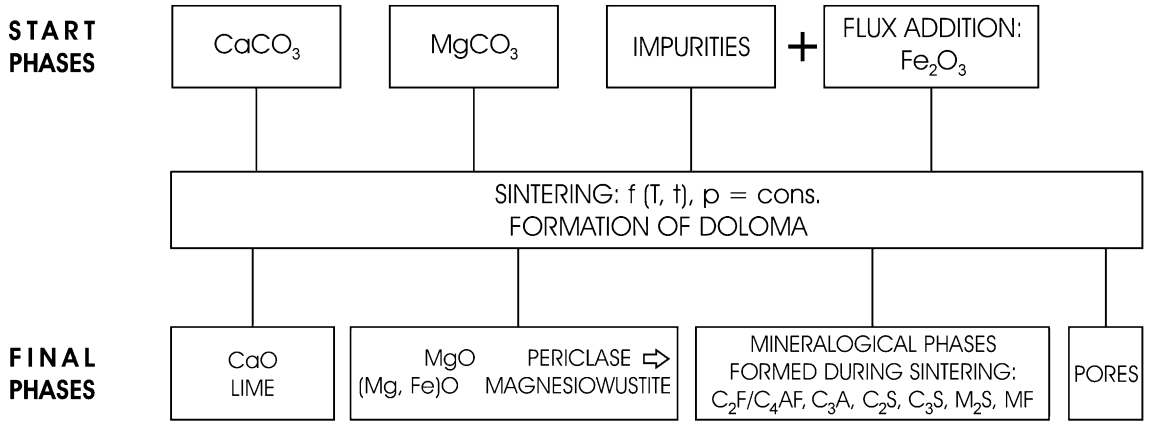

Fig. 1. Schematic microstructure development of dolomite with iron oxide addition during sintering.

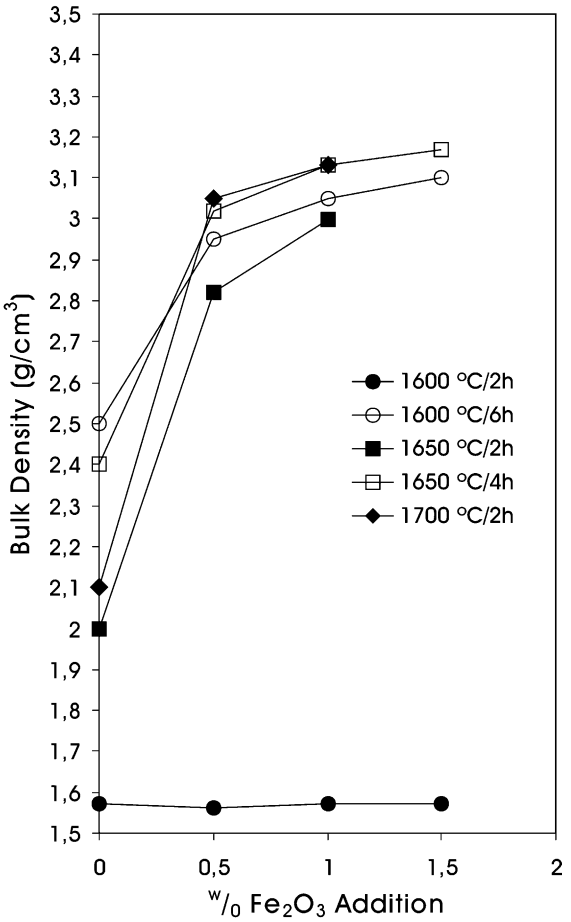

Fig. 2. The influence of iron oxide addition on the bulk density of the doloma studied [8].

rite etc., which stabilize the microstructure against hydration [4,5]. Iron oxide also has a beneficial effect on the bulk density [5–7]. In Fig. 2, the influence of the iron oxide addition on the bulk density is given [8].

Sintering of refractory materials, like dolomite, at high temperatures, is accompanied by grain growth of the phases MgO and CaO. In the literature, there are many studies concerning the grain growth of pure lime [9–11], pure periclase [11–13] and synthetic and natural doloma [14,15]. Reported values for kinetic exponents vary from 2 to 8 and values for activation energies of grain growth of CaO and MgO vary from about 100 to 600 kJ/mol, although the differences in chemical compositions and processing conditions are small.

Measurement of the grain growth is essential for calculation of the kinetic exponent and the activation energy. In this study, an attempt is made to determine the grain size of MgO with a scanning electron microscope in material contrast mode to get a higher resolution than the optical microscope [16,17].

2. Experimental

The starting material was a natural dolomite from Sille-Ecmel quarry deposit in Selcuklu-Konya, Turkey. In Table 1, the chemical composition of the raw dolomite is given. The material was crushed to smaller sizes and the material used in this study was taken from the fraction 3–6 mm in size. The measured decomposition temperature was about 950 °C for $CaCO_3$ and

Table 1
The chemical composition of the dolomite used in this study

Chemical composition [wt.%] (without loss of ignition)				
CaO	MgO	Fe_2O_3	Al_2O_3	SiO_2
56.3	43.0	0.1	0.3	0.3

800 °C for $MgCO_3$ [8]. For comparison purposes up to 1.5 wt.%, Fe_2O_3 (mill scale of size under 45 μm from KARDEMIR steelworks) was mixed in with the material as a sintering additive. The loose powders were sintered at temperatures 1600–1700 °C for 2 to 6 h. The tests were performed in air in a laboratory furnace with $MoSi_2$ heating elements.

The sintered doloma pieces were mounted in acrylic resin and then ground with SiC from 320 to 1000 grit and ethyl alcohol. The polishing of the specimen was done with 3 μm diamond paste. During the specimen preparation, no water was used because the lime phase rapidly hydrates, causing cracks in the lime grains of the doloma microstructure. For the mixture with mill scale, distilled water was used as binder [7] and the mixtures were dried at 110 °C for 2 h. For the determination of the distribution of phases with minor volume fraction, etched structures were also studied. Etching was done with pure acetic acid.

For the phase determination, XRD (from Philips, model PW1710) was used. In addition, EDX analyses were performed to obtain the chemical composition of the phases. The images were taken by scanning electron microscopy (SEM) from JEOL (model JSM 5410 LV), which was equipped with an EDX spectrometer from IXPF Systems (model 5480). This new generation SEM allows imaging at lower accelerating voltages with sufficient S/N ratio, which also reduces the information depth, when imaging with material contrast. Imaging has been performed at 15 kV. Because of the stronger contrast development, backscattered electron (BSE) material contrast was used for imaging of polished doloma specimens, instead of material contrast of secondary electrons (SEs). In the first run of experiments, only the MgO phase was quantitative-metallographically analysed. Automatic image analysis was performed, with Leica Quantimet 501 image analyser, on 4–12 images, depending on the magnification, where 600–850 particles were analysed for each sintering condition. Grains were manually separated only in cases, where the adjacent MgO grains were just at the early stages of neck formation.

3. Results and discussion

Fig. 3 shows an example of doloma with 0.5% Fe_2O_3 addition sintered at 1650 °C for 4 h with the

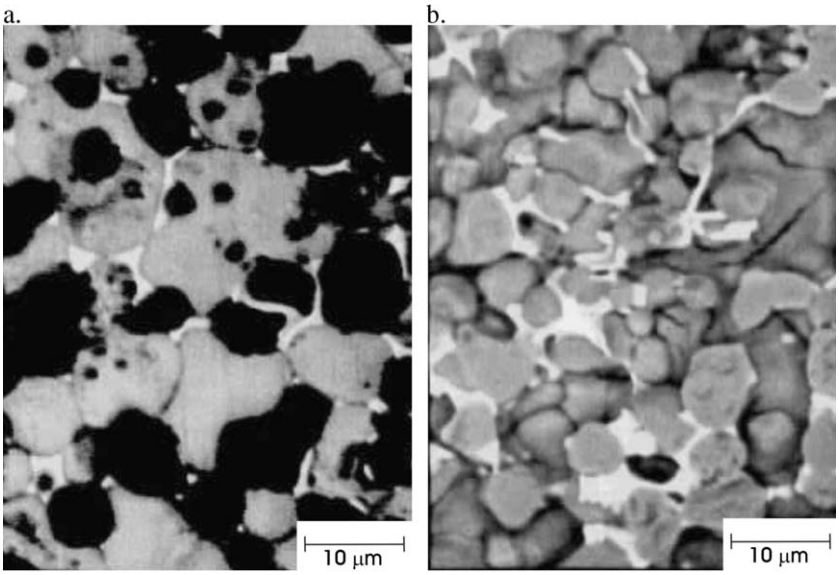

Fig. 3. Doloma with 0.5 wt.% Fe_2O_3 addition; sintered at 1650 °C for 4 h; (a) polished specimen; BSE material contrast; (b) etched specimen; SE topography contrast.

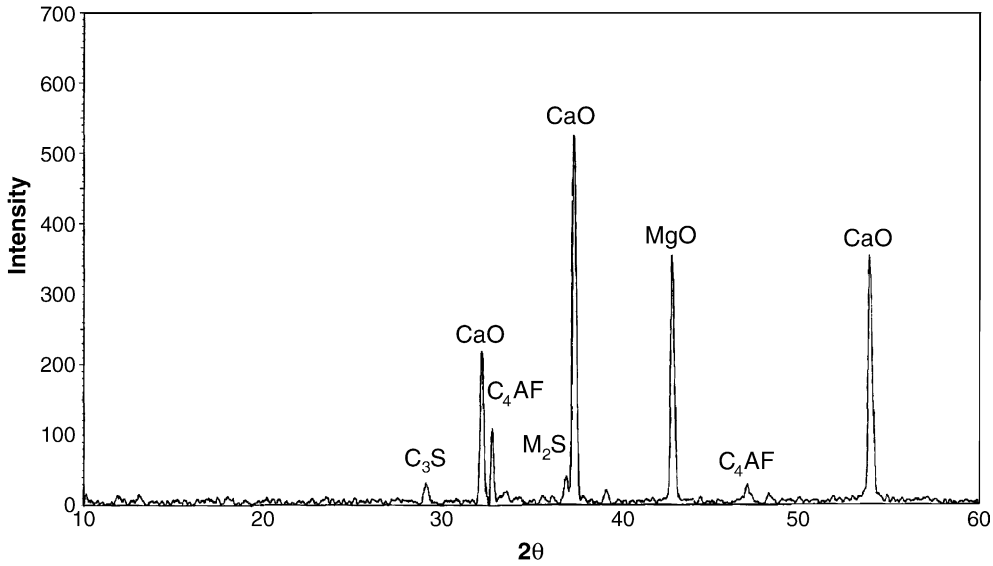

Fig. 4. XRD spectrum of the doloma with 0.5 wt.% Fe_2O_3 addition; sintered at 1650 °C for 4 h.

contrasts developed in the SEM. Fig. 3a gives the contrasts for different phases after firing. Lime with a higher mean atomic number appears as light grey and periclase with a lower mean atomic number is dark grey. In the grain boundaries and at triple junctions, a very light phase appears. Some grey phases are also seen. The figure demonstrates newly formed phases having a good wetting behaviour on lime and

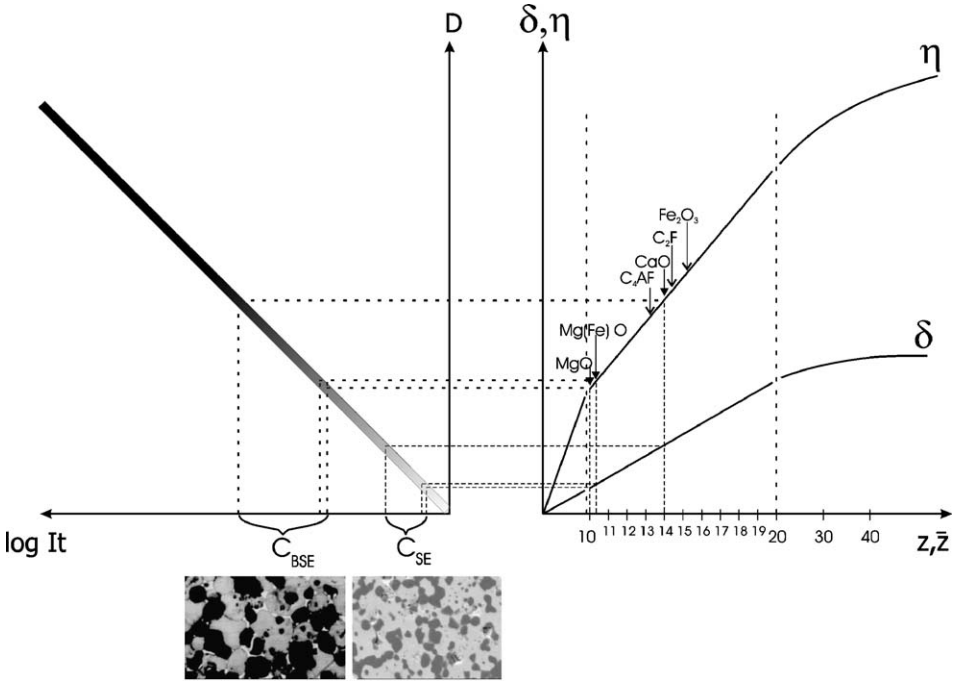

Fig. 5. SEM material contrast conditions for SE and BSE and the resulting phase contrasts.

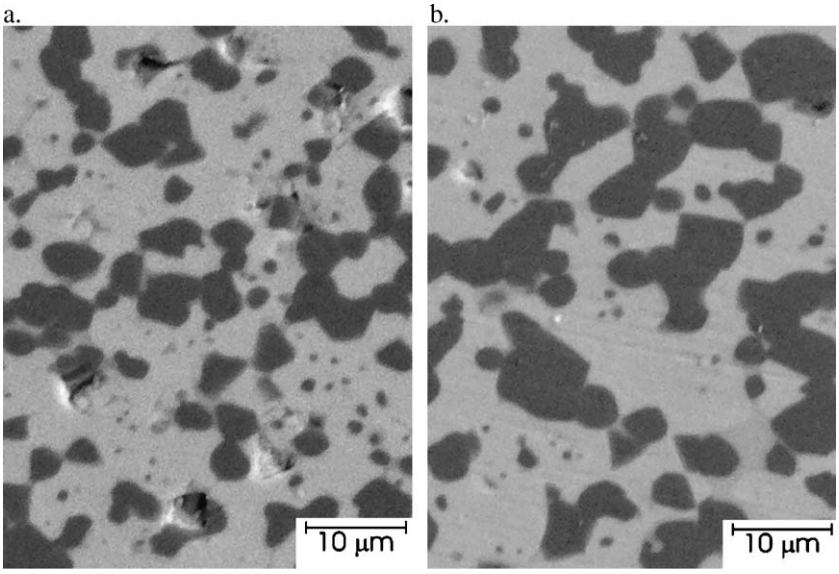

Fig. 6. As-received dolomite, after sintering for 6 h in the given condition. (a) Sintering temperature: 1600 °C. (b) Sintering temperature: 1650 °C.

periclase phases. All these grain boundary phases are the result of liquid phase sintering [18].

To get an idea of the spatial distribution of the minor phases formed during sintering, etching of the microstructure was performed (Fig. 3b). Despite the good wettability of the newly formed phases, the Fe_2O_3 addition of 0.5% is low enough so that only some minor fraction of the grain boundaries are covered.

The XRD and EDX analyses reveal that these phases form mainly due to the iron oxide additions. In Fig. 4, the XRD spectrum of this specimen is given. It can be seen that some phases of the system $CaO–MgO–SiO_2–Al_2O_3–Fe_2O_3$ are formed in minor

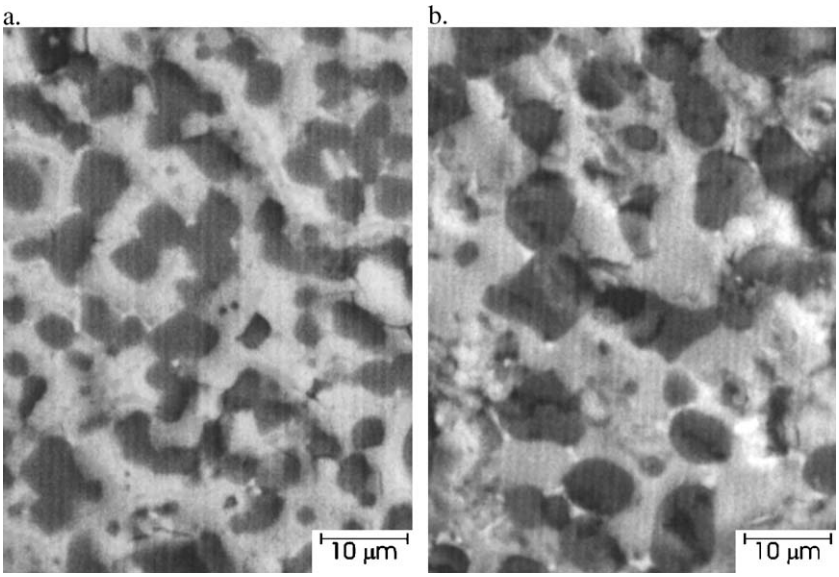

Fig. 7. Dolomite with 0.5% iron oxide addition, after sintering at 1650 °C in the given condition. (a) Sintering time: 2 h. (b) Sintering time: 6 h.

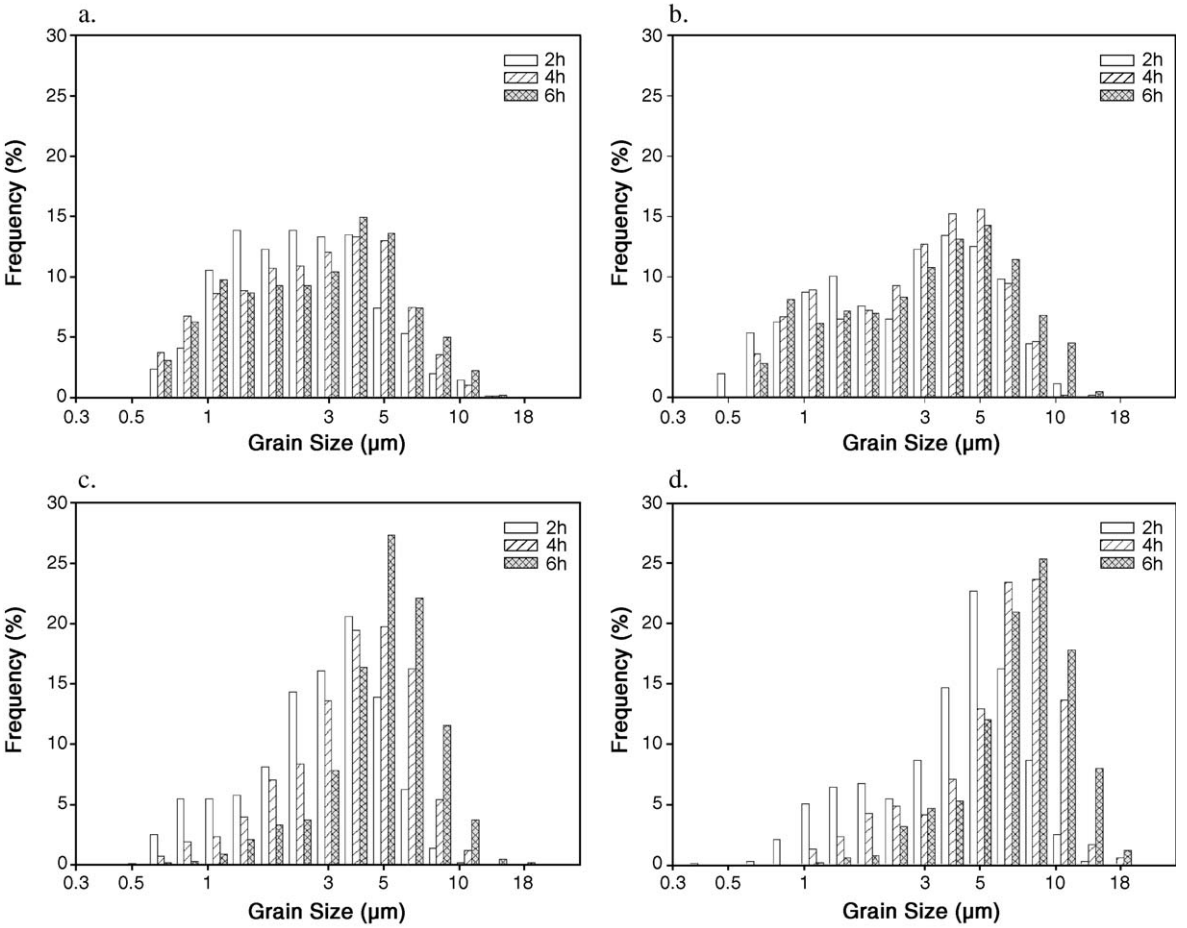

Fig. 8. Influence of the sintering time; (a) as-received dolomite, 1600 °C; (b) as-received dolomite, 1650 °C; (c) dolomite with 0.5% iron oxide addition, 1600 °C; (d) dolomite with 0.5% iron oxide addition, 1650 °C.

quantities. EDX analysis of these phases is not trivial because the information depth of X-rays compared to the size of these phases is high enough to be blunted by the main phases lime (CaO) and periclase (MgO). Only with the lime and periclase phases can reliable EDX analysis be performed. Both phases show minor additions of the elements given in the multicomponent system. Periclase (MgO) saturation with iron becomes higher with increasing Fe_2O_3 fraction added to the dolomite and periclase becomes magnesiowustite [(Mg, Fe)O]. The iron content of the magnesiowustite phase seems to be a function of the iron oxide fraction in the mixture [8].

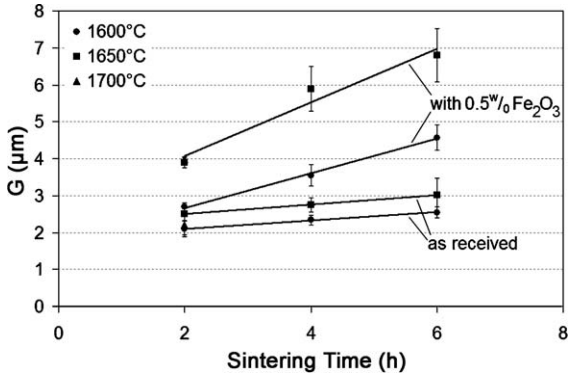

Fig. 9. The influence of sintering time on the grain growth of periclase in the dolomite as received and with 0.5% iron oxide addition after various sintering temperatures.

Table 2
Results of the image analysis performed

Samples			Median grain size (μm)	F2F[a] standard deviation (±)
As received	1600 °C	2 h	2.09	0.21
		4 h	2.34	0.13
		6 h	2.54	0.15
	1650 °C	2 h	2.51	0.19
		4 h	2.75	0.20
		6 h	3.02	0.45
	1700 °C	2 h	2.21	0.27
With 0.5 wt.% Fe_2O_3	1600 °C	2 h	2.69	0.11
		4 h	3.55	0.29
		6 h	4.57	0.34
	1650 °C	2 h	3.89	0.14
		4 h	5.89	0.61
		6 h	6.80	0.72
	1700 °C	2 h	3.98	0.10

[a] An abbreviation for the Frame-to-Frame term.

The contrast developed in the SEM on the imaging of the polished specimen are given in Fig. 5. In the diagram at the right hand of the figure, the relationship between electron yield (δ for SE, η for BSE) and atomic number and also mean atomic number are given. The main phases, lime (CaO), periclase (MgO) and magnesiowustite [(Mg, Fe)O], as well as some minor phases, are shown on this diagram by their mean atomic numbers. The contrasts developed are shown on the density-exposure diagram, where the density curve is given for γ=1. As can easily be seen in the images below the curve, where also the contrast, C, is given for BSE and SE, the contrast in the BSE image is higher compared to the SE image without visible resolution losses.

In Figs. 6 and 7, some relevant microstructures of the image analyses accomplished are given. Fig. 6 shows the as-received dolomite microstructures after sintering at temperatures 1600–1650 °C for 6 h. The temperature effect on the grain growth of MgO is obvious. Fig. 7 shows the dolomite microstructures with 0.5% iron oxide addition after sintering at 1650 °C for 2 and 6 h. Here, the effect of sintering time on the grain growth of MgO is also pronounced. The images in both structures demonstrate that this two-phase microstructure lime, being the majority phase, takes the role of the matrix, and periclase, being the minority phase, is distributed randomly in the matrix. Thus, if the diffusional relationship is considered, it should be kept in mind that the diffusion in the lime phase occurs in a different way than in the periclase phase. As a matrix, lime is continuous, whereas the diffusion in periclase also involves diffusional motion

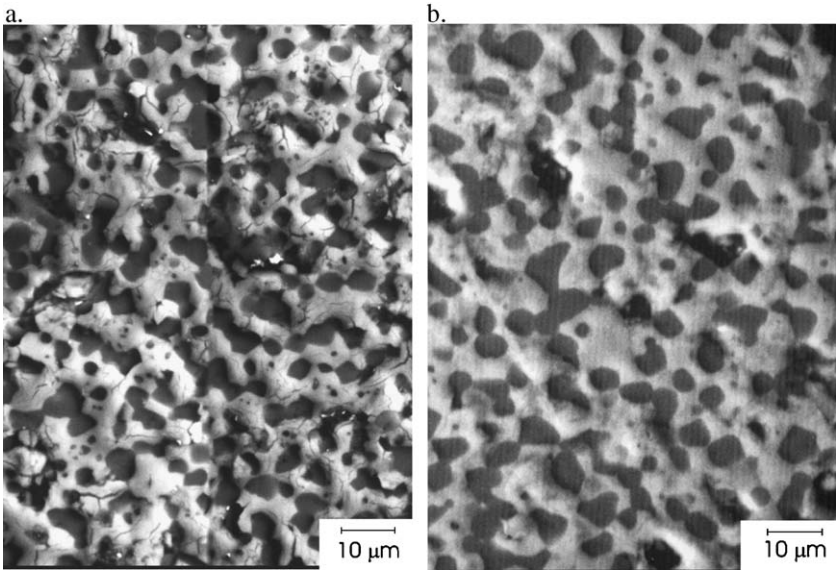

Fig. 10. Dolomite as received (a) and with 0.5% iron oxide addition (b), after sintering in the given condition. (a) As received; 1700 °C for 2 h. (b) With 0.5% iron oxide; 1700 °C for 2 h.

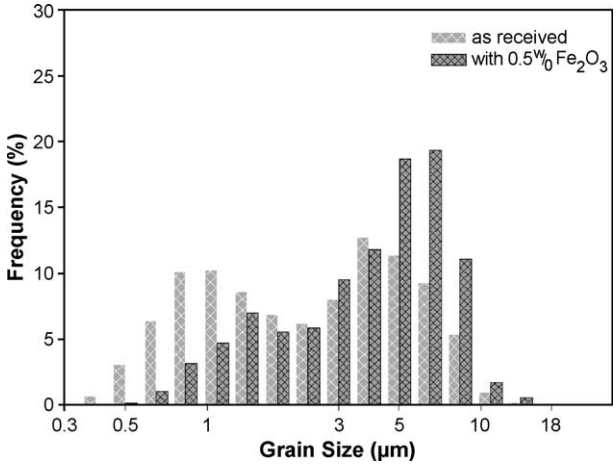

Fig. 11. The influence of 0.5% iron oxide addition on the grain growth of periclase in the dolomite during sintering at 1700 °C for 2 h.

in lime as the periclase phase is discontinuous to a high degree.

In Fig. 8, the resulting MgO grain size distributions for dolomite in the as-received condition (Fig. 8a and b) and dolomite with 0.5% iron oxide addition (Fig. 8c and d) are given, where the distribution histograms are arranged by increasing sintering time. The distribution histograms show little effect of the sintering time for as-received dolomite, whereas the differences are more pronounced for dolomite with 0.5% iron oxide addition. To get a better insight, the influence of sintering time on the grain growth of periclase in the dolomite in the as-received condition and with 0.5% iron oxide addition after various sintering temperatures are shown in Fig. 9. Here, the measured median grain size data, which are given in Table 2, for the whole specimen and sintering conditions studied, are used. From this figure, it can easily be seen that the iron oxide addition accelerates the grain growth of the MgO phase.

The results for the highest sintering temperature, 1700 °C for 2 h, are presented in Fig. 10, where the images of the microstructures of the as-received domonite and dolomite with 0.5% iron oxide addition are set against each other. The relevant MgO grain size distributions are given in Fig. 11. Sintering results in a more pronounced grain growth of the periclase phase when iron oxide is added. With this addition, the bimodality in the size distribution of periclase in the as-received dolomite also disappears.

In Fig. 12, the influence of the sintering temperature on the grain growth of periclase in dolomite is given. Here, again, the same role of the iron oxide addition on the MgO grain growth is seen. With increasing sintering temperature, the liquid phase sintering due to iron oxide addition accelerates the MgO grain growth. MgO grains of the doloma in the as-received condition are largely unaffected by an increase in the sintering temperature.

The kinetics of the grain growth for the single-phase microstructure is given by the rate equation [19–21]:

$$G_n - G_0^n = K_0 t e^{-\frac{Q}{RT}} \quad (1)$$

where G is the average grain size, G_0 is the average grain size at time zero, n is the kinetic exponent for grain growth and Q is the activation energy for grain growth.

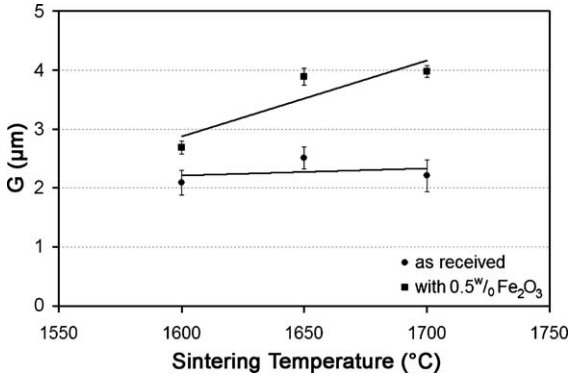

Fig. 12. Influence of the sintering temperature on the grain growth of periclase in dolomite.

If G_0 is small enough compared to the final G, this term can be neglected (which is true for the case studied [14]):

$$G^n = K_0 t e^{-\frac{Q}{RT}} \tag{2}$$

$$\log(G^n/t) = \log K_0 - \frac{Q}{2.303R}\cdot\frac{1}{T} \tag{3}$$

The plot of $\log(G^n/t)$ vs. $1/T$, with a slope of $-Q/2.303R$ enables the calculation of the activation energy of the isothermal heat treatment. The determination of the kinetic exponent, n, is a consequence of Eq. (2); the slope of the straight line in the diagram log G vs. log t gives the value of $1/n$.

Values calculated for these two important parameters, the kinetic exponent, n (which is correlated to the rate-controlling mechanism of grain boundary migration), and the activation energy, Q (which is correlated to the elementary mass transport during isothermal annealing), are represented in Figs. 13 and 14. The log G vs. log t diagram for the determination of the kinetic exponent of the MgO grain growth shows two different slopes for the two sintering temperatures studied (Fig. 13). Doloma in the as-received condition has n values of 5.7 and 6.1, which indicates a kinetic exponent of 6. In the doloma with 0.5% Fe_2O_3 addition, the n values for the two temperatures are 1.9 and 2.1, so that the kinetic exponent is expected to be 2. The dramatic drop from 6 to 2 in the kinetic exponent value with a minor iron oxide addition of 0.5% causes the MgO grains to be destabilized, and grain growth is accelerated.

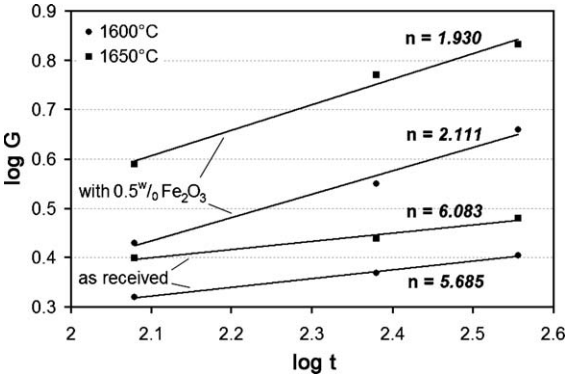

Fig. 13. Calculation of the kinetic exponent, n.

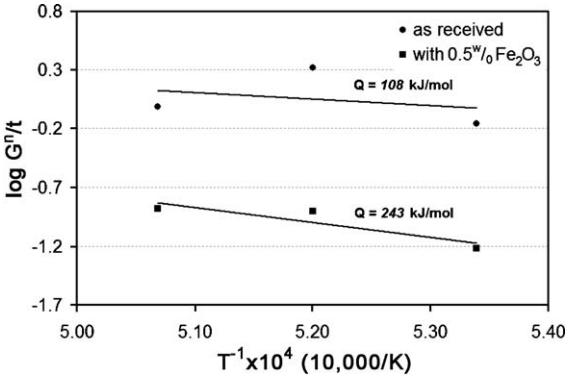

Fig. 14. The activation energy plot for dolomite in as-received condition and for dolomite with 0.5% iron oxide addition.

In Fig. 14, plots of the activation energy for the MgO grain growth process in the as-received dolomite and for dolomite with 0.5% iron oxide addition are given. The regression analysis yields an activation energy of 243 kJ/mol for the periclase grain growth in the as-delivered state and an activation energy of 108 kJ/mol for the periclase grain growth in doloma with 0.5% Fe_2O_3 addition.

4. Conclusions

(1) An iron oxide addition in the form of mill scale does not only cause a strong densification due to liquid phase sintering, where a rearrangement of the grains is easily obtained but it also does form various grain boundary phases, like dicalciumferrite, tetracalciumaluminoferrite, etc. After sintering, some iron is also found in the periclase (MgO), so that the phase becomes magnesiowustite [(Mg, Fe)O], which introduces the destabilization of the periclase phase.

(2) In the doloma studied, the following grain growth laws were determined:

For the material in as-received state:

$$G^6 = K_0 t e^{-\frac{108}{RT}}$$

For the material with 0.5% Fe_2O_3 addition:

$$G^2 = K_0 t e^{-\frac{243}{RT}}$$

Acknowledgement

The authors acknowledge the support of Dr. R.H. Özsahin, General Director of Konya Selcuklu Chrome-Magnesite Brick Ind., and are grateful for the supply of the dolomite.

References

[1] Trojer F. Mineralogie basissche feurfest-produkte. New York: Springer-Verlag; 1981. p. 42.
[2] Meyer W, Franchi A, Buchebner G, Willingshofer M. The use of dolomite–carbon-lined ladless for the production of super-clean steels. Veitsch-Radex Rundsch 1998;2:32–44.
[3] Ghosh A. Secondary steelmaking: principles and applications. Boca Raton: CRC Press; 2001. p. 275.
[4] Schlegel E. Sintering of dolomite as a function of the raw material properties. Sprechsaal 1987;120(3):170–6.
[5] Serry MA, Mandour MA, Osman AGM, Girgis LG. Effect of dopants on the microstructure and properties of dolomitic magnesite. Interceram 1996;45(3):162–5.
[6] Antonov GI, Grivakova ZA. Sintering and hydration resistance of dolomites from the Zavadovsk deposits. Refract Ind Ceram 1988;6:357–60 [Translated from Ogneupory].
[7] Koval EJ, Messing GL, Bradt R. Effects of raw material properties and Fe_2O_3 additions on the sintering of dolomites. Ceram Bull 1984;63(2):274–7.
[8] Yeprem HA. Characterisation of Sintering of a Local Dolomite for Production of Dolomite Refractory, PhD thesis, Yildiz Technical University, Istanbul, Turkey; 2003.
[9] Yasuda E, Ramesh KS, Bao QL, Kimura S. Decrease and pore growth during post sintering. Presented at the Ceramics Microstructure Symposium, UC, Berkeley, USA, July; 1986.
[10] Rice RW. CaO: II. Properties. J Am Ceram Soc 1969;52(8):428–36.
[11] Daniels AU, Lowrie RC, Gibby RL, Cutler IB. Observations on normal grain growth of magnesia and calcia. J Am Ceram Soc 1962;45(6):282–5.
[12] Spriggs RM, Brissette LA, Vasilos T. Grain growth in fully dense magnesia. J Am Ceram Soc 1964;47(8):417–8.
[13] Nicholson GC. Grain growth in magnesium oxide containing iron oxide or titanium dioxide. J Am Ceram Soc 1966;49(1):47–9.
[14] Baldo JB, Bradt RC. Grain growth of the lime and periclase phases in a synthetic doloma. J Am Ceram Soc 1988;71(9):720–5.
[15] Fonseca AT, Vieria JM, Baptista JL. Grain growth in synthetic and natural dolomas. Ceram Int 1998;24:163–73.
[16] Karagöz S, Fischmeister H. Quantitative metallography of high speed steels by SEM. Steel Res 1987;1:46–51.
[17] Bischoff E, Opielka H, Kabyemera I, Karagöz S. SEM-investigations into the quantitative metallographical determination of carbides in high speed steels. Prakt Metallogr 1995;2:77–89.
[18] White J. Magnesia–based refractories. In: Alper MA, editor. High temperature oxides: Part I. Magnesia, lime and chrome refractories. New York: Academic Press; 1970. p. 118–9.
[19] Brook RJ. Controlled grain growth. In: Wang FF, editor. Treatise on materials science and technology. Ceramic Fabrication Processes, vol. 9. New York: Academic Press; 1976. p. 331–64.
[20] Hillert M. On the theory of normal and abnormal grain growth. Acta Metall 1965;13(4):227–38.
[21] Glaeser AM. Microstructural developments in ceramics—the role of grain growth. Yogyo Kyokaishi 1984;92(10):538–46.